Astron. Astrophys. 325, 318–328 (1997)

ASTRONOMY
AND
ASTROPHYSICS

Wave heating of coronal loops driven by azimuthally polarised footpoint motions

I. Stationary behaviour in dissipative MHD

D. Berghmans* **and W.J. Tirry***

Centre for Plasma Astrophysics, K.U. Leuven, Celestijnenlaan 200 B, B-3001 Heverlee, Belgium

Received 17 January 1997 / Accepted 10 March 1997

Abstract. We study the heating of coronal loops by linear resonant Alfvén waves that are excited by photospheric footpoint motions of the magnetic field lines. The analysis is restricted to azimuthally polarised footpoint motions so that Alfvén waves are excited. At the radii where Alfvén waves, travelling back and forth along the loop, are in phase with the footpoint motions the oscillations grow unbounded in ideal MHD. Inclusion of dissipation prevents singular growth and we can look at the steady state in which the energy input at the photosphere is balanced by the energy dissipated at the resonance.

The crux of our study is that the azimuthal wave number is taken non-zero which means that also fast waves, including quasi-modes, can be excited by the purely azimuthally polarised footpoint motions. In this case resonant Alfvén waves are not only excited directly by the footpoint motions but also indirectly through coupling to fast waves. For some footpoint motions these contributions counteract each other leading to virtually no heating (anti-resonance) while for values corresponding to a quasi-mode the two contributions act in concert leading to enhanced heating. This dramatic influence of the quasi-mode is unexpected since, in contrast to a sideways driven loop, a loop driven at the footpoints by azimuthally polarised footpoint motions does not need quasi-modes as energy carrier waves.

In this paper a stationary state is assumed which allows us to determine the optimal footpoint characteristics for heating, but does not give any information on the time scales involved. This item is adressed in a companion paper where an identical system is studied time dependently using ideal MHD. This twin study investigates the attainability of the heating scenarios and provides an enhanced insight in the results of the present paper.

Key words: MHD – Sun: corona; oscillations – waves – methods: analytical

Send offprint requests to: D. Berghmans

* Research Assistant of the FWO-Vlaanderen

1. Introduction

High resolution observations from space and from the ground give overwhelming evidence that the solar corona is a highly inhomogeneous plasma which is structured by the ubiquitous magnetic field. Since Skylab it is known that the largest contribution to the X-ray emission and to the heating of the solar corona comes from loop like structures in the solar atmosphere. The magnetic loops are viewed as the basic magnetic building blocks of the solar corona. The high conductivity and the relatively high mass density of the photospheric plasma provide an effective photospheric anchoring of the magnetic field lines. The photospheric footpoints of the magnetic field lines are forced to follow the convective motions of the photospheric plasma.

If the motions of the footpoints of the magnetic field lines have time scales at least of the order of the Alfvénic transit time, fast and slow magnetosonic waves and Alfvén waves are generated. Due to the steep density gradients at the photospheric edges these MHD waves are reflected back and forth along the length of the loop. The loop then acts as a leaking, resonant cavity for MHD waves which can be dissipated by various mechanisms which create small length scales and hence heat the loop. This scenario is supported by recent observations: Ulrich (1996) reported magnetic oscillations in the photosphere which were identified as outgoing Alfvén waves with substantial power at low frequencies, while soft X-ray lines from the XRP indicate nonthermal motions of 30-40 km/s above active regions (Saba & Strong 1991). However, the observations so far are not sufficiently detailed to either exclude or confirm the generation of large enough wave fluxes in the photosphere (Zirker, 1993).

An important property of MHD waves in an inhomogeneous plasma is that individual magnetic surfaces can oscillate with their own Alfvén frequencies. In ideal linear MHD this can happen without interaction with neighbouring magnetic surfaces. These local Alfvén oscillations are polarized in the magnetic surfaces and perpendicular to the magnetic field lines. Dissipative effects produce coupling to neighbouring surfaces. For large values of the viscous and magnetic Reynolds numbers as in the

solar corona the local Alfvén oscillations are still characterized by steep gradients across the magnetic surfaces. Excitation of these local Alfvén oscillations provides a way to dissipating wave energy efficiently. This can be achieved in a first scenario by means of a sideways impinging MHD wave and in a second scenario by driving at the footpoints of the magnetic fieldlines of the loop.

In the first scenario, the sideways impinging MHD wave must necessarily be a fast wave since Alfvén waves cannot transport energy perpendicular to the magnetic flux surfaces and slow waves are negligible due to the low gas pressure in the solar corona. At the magnetic surface where the frequency of the impinging fast wave matches the local Alfvén frequency, local resonant Alfvén waves are excited. In this process, called resonant absorption, the fast wave transfers energy across the magnetic surfaces up to the resonant surface. In this scenario the excitation of the localised oscillations is indirect since we need fast magnetosonic waves that propagate across the magnetic surfaces to excite them. Due to the small length scales thus generated, dissipation is enhanced by several orders of magnitude over its classical value in a uniform plasma (Kuperus, Ionson & Spicer 1981; Davila 1987; Hollweg 1990, 1991; Goossens 1991). Sideways excitation is most efficient when driving at a frequency of a fast eigenmode of the global loop structure, which falls into the Alfvén continuum. In dissipative MHD these modes are recovered as eigenmodes which are exponentially damped in time. Due to their global character (oscillating with the same frequency throughout the plasma) these modes are called 'global modes'. For ideal MHD such a damped oscillation cannot be an eigenmode of the system, and for this reason they are often called 'quasi-modes' (Ofman, Davila & Steinolfson 1995; Wright & Rickard 1995; Tirry & Goossens 1996). A second scenario for the excitation of localised Alfvén oscillations involves driving at the photospheric footpoints of the magnetic field lines. This problem involves the explicit solution of the wave-dynamics not only in the radial direction, but also in the longitudinal direction in order to include the appropriate boundary conditions at the loop's feet. Due to the intrinsic difficulty of the footpoint driven problem, authors have often assumed the azimuthal wave number to be zero (Heyvaerts & Priest 1983; Berghmans & De Bruyne 1995; Berghmans, De Bruyne & Goossens 1996; Poedts & Boyton 1996; Ruderman et al. 1996). A remarkable exception to this restriction has been the work of Halberstadt & Goedbloed (1995a,b). They calculated the stationary state solutions excited by footpoint motions normal to the magnetic surfaces having a non-zero divergence and a non-zero vorticity.

The main objective of this study is to extend the above mentioned investigations of wave heating of coronal loops to the case where the azimuthal wave number is taken non-zero which means that also fast waves can now be excited with the purely azimuthally polarised footpoint motions, including the quasi-modes. In this case resonant Alfvén waves are not only excited directly by the footpoint motions but also indirectly through coupling to fast waves. Which of these two contributions is dominant and whether they reinforce each other or counteract (anti-resonance) turns out to depend crucially on the (ω_d, k_y) value as compared to (ω_q, k_y) of a nearby quasi-mode. We interpret this behaviour in terms of energy fluxes going in *and out* the dissipative layer. This dramatic influence of the quasi-mode is unexpected since, in contrast to a sideways driven loop, a loop driven at the footpoints by azimuthally polarised footpoint motions does not need the quasi-modes as energy carrier waves. In this paper a stationary approach is adopted which allows us to study the steady state of a coronal loop which is driven by azimuthally polarised footpoint motions, but does not give any direct information on the time scales involved. This question is adressed in a companion paper (Tirry & Berghmans 1997, hereafter referred to as paper II) where an identical system is studied but using a time-dependent, ideal approach. This twin study then investigates the attainability of the heating scenarios presented in this paper and provides an enhanced understanding of the anti-resonance.

The paper is organized as follows. In the next section the relevant equations, the boundary conditions and the underlying assumptions are discussed. In Sect. 3 we solve the mathematical problem in three stages. Inspired by Ruderman et al. (1996) we take up the driving footpoint motion as a source term in our equations and write the solutions as a Fourier superposition of sines in the z-direction (Sect. 3.1). We then obtain an infinite set of ordinary differential equations governing the corresponding Fourier coefficients. Most of these equations are non-resonant and can be solved by direct numerical integration of the ideal equations (Sect. 3.2). However when the frequency of the driving footpoint motions matches the local Alfvén frequency at a position x_A, a resonant contribution is encountered. To calculate such a Fourier coefficient, viscosity and resistivity need to be included which remove the singularity. This is done in Sect. 3.3 where we follow an elegant method based on Goossens, Ruderman & Hollweg (1995). In Sect. 4 we derive an expression for the Poynting flux through the photosphere as a function of the wave-amplitude found in Sect. 3. This turns out to be a valuable tool when interpreting the results in Sects. 5 and 6. Finally in Sect. 7 we give a summary and discussion.

2. Physical model

A coronal loop is modelled as a static, straight plasma slab with thickness a, obeying the standard set of the visco-resistive MHD equations in which gravity is ignored. In our Cartesian coordinate system the x-coordinate corresponds to the radial direction, the y-coordinate to the (ignorable) azimuthal coordinate and the z-coordinate represents the direction along the loop.

At $z = 0$ we impose a given footpoint motion whereas at $z = L$ we assume the loop to be held immovable. This can be done without any loss of generality because of the principle of superposition for solutions of linear equations. The boundary planes model the sharp transition from the corona to the photosphere (i.e. transition region, chromosphere and photosphere). We shall refer to these boundary planes as the 'photospheric edges' of the loop and we implicitly assume that a disturbance initiated in the photosphere indeed reaches the corona. In the ra-

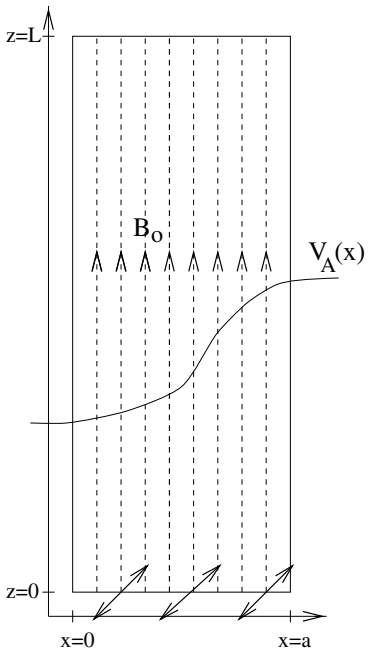

Fig. 1. A cartoon of the configuration used to model a coronal loop.

dial direction we assume for mathematical tractability rigid wall conditions at $x = 0$ and $x = a$. We view $x = 0$ as the interior of the loop and $x = a$ as the exterior coronal environment.

The plasma is permeated by a uniform magnetic field ($\mathbf{B_0} = B_0\mathbf{e_z}$) and has a uniform pressure p_0 which we neglect in comparison with the magnetic pressure. Inhomogeneity of the plasma is introduced by a continuously varying density

$$\rho_0(x) = \rho_A + \rho_B \cos(\frac{\pi}{a}x) \qquad \text{with} \qquad \rho_B < \rho_A, \tag{1}$$

which models the higher density inside the loop. Fig. 1 shows a cartoon of the configuration used to model a coronal loop.

Since we did not take into account a z-dependence of the density, our analysis is to be applied only to coronal loops with their apex lower than one scale height.

The plasma is being shaken by small-amplitudes perturbations at the footpoints of the magnetic field lines on the $z = 0$ plane. After linearisation, the visco-resistive MHD equations can be reduced for a pressureless plasma to

$$\{\frac{1}{v_A^2}\frac{\partial^2}{\partial t^2} - \frac{\partial^2}{\partial z^2} - \frac{\partial^2}{\partial x^2} - \frac{(\eta+\nu)}{v_A^2}\frac{\partial^3}{\partial x^2\partial t}\}\xi_x = \frac{\partial^2\xi_y}{\partial y\partial x}, \tag{2}$$

$$\{\frac{1}{v_A^2}\frac{\partial^2}{\partial t^2} - \frac{\partial^2}{\partial z^2} - \frac{\partial^2}{\partial y^2} - \frac{(\eta+\nu)}{v_A^2}\frac{\partial^3}{\partial x^2\partial t}\}\xi_y = \frac{\partial^2\xi_x}{\partial y\partial x}. \tag{3}$$

where ξ is the Lagrangian displacement and the Alfvén speed v_A is given by

$$v_A(x) = \sqrt{\frac{B_0^2}{\mu\rho_0(x)}}.$$

The coupled system of partial differential equations (2) and (3) in ξ_x and ξ_y describes coupled fast-Alfvén waves. Note that the (scalar) viscosity η and resistivity ν are only retained in terms where they are multiplied with derivatives in the inhomogeneous x-direction. The reason for doing so is that in the solar corona these dissipative effects are extremely small and an ideal description is very adequate almost everywhere. However, in what follows we shall see that an ideal description leads to infinite radial gradients. We have anticipated this problem encountered in ideal MHD by including viscosity and resistivity anyway, but only in terms where they are multiplied by radial derivatives of perturbed quantities. Slow waves are absent ($\xi_z = 0$) because the plasma pressure was neglected. Total pressure is given by

$$P = -\frac{B_0^2}{\mu}(\frac{\partial\xi_x}{\partial x} + \frac{\partial\xi_y}{\partial y}) \tag{4}$$

Since the equilibrium quantities are constant in the y-coordinate which runs over an infinite domain, we can Fourier analyse with respect to y. For the Fourier component corresponding to the wave number k_y, the time evolution and the spatial variation in x and z are described by

$$\{\frac{1}{v_A^2}\frac{\partial^2}{\partial t^2} - \frac{\partial^2}{\partial z^2} - \frac{\partial^2}{\partial x^2} - \frac{(\eta+\nu)}{v_A^2}\frac{\partial^3}{\partial x^2\partial t}\}\xi_x = ik_y\frac{\partial\xi_y}{\partial x}, \tag{5}$$

$$\{\frac{1}{v_A^2}\frac{\partial^2}{\partial t^2} - \frac{\partial^2}{\partial z^2} + k_y^2 - \frac{(\eta+\nu)}{v_A^2}\frac{\partial^3}{\partial x^2\partial t}\}\xi_y = ik_y\frac{\partial\xi_x}{\partial x}, \tag{6}$$

and total pressure is given by

$$P = -\frac{B_0^2}{\mu}(\frac{\partial\xi_x}{\partial x} + ik_y\xi_y). \tag{7}$$

Tirry, Berghmans & Goossens (1997) studied the generation of linear MHD waves satisfying the ideal version of Eqs. (5) and (6). However, these authors considered only radially polarised footpoint motions so that the resonant Alfvén waves are indirectly driven through coupling with the fast waves. Alternatively, also the generation of linear MHD waves satisfying Eqs. (5) and (6) by azimuthally polarised footpoint motions (8) has been studied before, but only for y-independent footpoint motions. In this case the fast and Alfvén waves are decoupled. Heyvaerts & Priest (1983) studied in this context the phase-mixing process while Berghmans & De Bruyne (1995) gave a fully analytical treatment of the time evolution of azimuthal Alfvén waves (corresponding to the ξ_y component as described by the ideal version of Eq. (6)). Ruderman et al (1996) then, looked at the stationary state of this process in which the energy injected at the photospheric part of the loop is balanced by the energy dissipated in the coronal part of the loop.

The present investigation can be seen as an extension of the work by Ruderman et al (1996). The important novelty is that the azimuthal wave number can be taken non-zero which leads to fascinating new physics: resonant Alfvén waves are now directly driven at the footpoints and indirectly through coupling with fast waves, especially with quasi-modes. We shall investigate the interplay of these two contributions in detail.

3. Mathematical approach

We take all length scales and time scales in the above expressions as being non-dimensionalised so that $v_A(x=0)=1$, $a=1$ and $\frac{B_0^2}{\mu}=1$. Note that this implies that $\rho_A+\rho_B=1$.

3.1. Handling the footpoint motions

We represent the footpoint motions by inhomogeneous boundary conditions for Eqs. (5) and (6) at the $z=0$ and the $z=L$ boundary planes:

$$\begin{aligned}\xi_x(x,y,z=0,t) &= 0,\\ \xi_x(x,y,z=L,t) &= 0,\\ \xi_y(x,y,z=0,t) &= R_y e^{i(k_y y-\omega_d t)},\\ \xi_y(x,y,z=L,t) &= 0.\end{aligned} \tag{8}$$

The footpoint motion is taken to be purely polarised in the azimuthal direction and, for simplicity, independent of x. In addition, we have taken an $e^{-i\omega_d t}$ time dependence of the footpoint motions since we look for stationary solutions. As a consequence, no initial conditions need to be provided. In paper II, x-dependent profiles R_y will be considered as well as an arbitrary time dependence.

In the present paper we investigate the stationary behaviour of the system determined by expressions (5), (6) and (8). This means that we assume that the footpoint motion has been driving the loop for a sufficiently long time so that all transient phenomena have vanished and an asymptotic state is attained where all variables oscillate with the frequency ω_d of the driving footpoint motions. Whether this stationary state is in practice attainable within a typical lifetime of a coronal loop, is looked at in more detail in paper II. By assuming the time dependence $e^{-i\omega_d t}$ for the perturbed quantities ξ_x and ξ_y we obtain

$$\{-\frac{\omega_d^2}{v_A^2}-\frac{\partial^2}{\partial z^2}-\frac{\partial^2}{\partial x^2}+\frac{i\omega_d(\eta+\nu)}{v_A^2}\frac{\partial^2}{\partial x^2}\}\xi_x = ik_y\frac{\partial \xi_y}{\partial x}, \tag{9}$$

$$\{-\frac{\omega_d^2}{v_A^2}-\frac{\partial^2}{\partial z^2}+k_y^2+\frac{i\omega_d(\eta+\nu)}{v_A^2}\frac{\partial^2}{\partial x^2}\}\xi_y = ik_y\frac{\partial \xi_x}{\partial x}. \tag{10}$$

With the aid of the function

$$\varphi(x,y,z)=\xi_y(x,y,z)-(1-\frac{z}{L})R_y e^{ik_y y}, \tag{11}$$

we include the footpoint motions as a driving term in the equations, while the boundary conditions become homogeneous

$$\begin{aligned}&\{-\frac{\omega_d^2}{v_A^2}-\frac{\partial^2}{\partial z^2}-\frac{\partial^2}{\partial x^2}+\frac{i\omega_d(\eta+\nu)}{v_A^2}\frac{\partial^2}{\partial x^2}\}\xi_x-ik_y\frac{\partial\varphi}{\partial x}=0\\ &\{-\frac{\omega_d^2}{v_A^2}-\frac{\partial^2}{\partial z^2}+k_y^2+\frac{i\omega_d(\eta+\nu)}{v_A^2}\frac{\partial^2}{\partial x^2}\}\varphi-ik_y\frac{\partial\xi_x}{\partial x}=\\ &\qquad(1-\frac{z}{L})(\frac{\omega_d^2}{v_A^2}-k_y^2)R_y.\end{aligned} \tag{12}$$

and

$$\xi_x(z=0)=0=\xi_x(z=L),\quad \varphi(z=0)=0=\varphi(z=L).$$

These homogeneous boundary conditions for ξ_x and φ now allow for the following sine-expansions

$$\begin{aligned}\xi_x(x,y,z) &= \frac{2}{L}\sum_{n=1}^{\infty}X^{(n)}(x,y)\sin(\frac{n\pi}{L}z),\\ \varphi(x,y,z) &= \frac{2}{L}\sum_{n=1}^{\infty}Y^{(n)}(x,y)\sin(\frac{n\pi}{L}z).\end{aligned} \tag{13}$$

Expansion of the function $(1-\frac{z}{L})$ in Eqs. (12) in a series of sines results in

$$1-\frac{z}{L}=\frac{2}{L}\sum_{n=1}^{\infty}\frac{L}{n\pi}\sin(\frac{n\pi}{L}z)\qquad \text{for}\ \ z\in]0,L], \tag{14}$$

where the righthandside is convergent to the lefthandside for all values of z but $z=0$. This poses no difficulties since we only look for a weak solution in what follows. With the use of the sine-transforms the coupled partial differential Eqs. (12) are replaced by an infinite set of coupled ODE for $X^{(n)}$ and $Y^{(n)}$. There is no coupling between Fourier coefficients $X^{(n)}$ and $Y^{(n)}$ for different n.

$$\begin{aligned}&\{-\frac{\omega_d^2}{v_A^2}+(\frac{n\pi}{L})^2-\frac{\partial^2}{\partial x^2}+\frac{i\omega_d(\eta+\nu)}{v_A^2}\frac{\partial^2}{\partial x^2}\}X^{(n)}\\ &=ik_y\frac{\partial Y^{(n)}}{\partial x}\end{aligned} \tag{15}$$

$$\begin{aligned}&\{-\frac{\omega_d^2}{v_A^2}+(\frac{n\pi}{L})^2+k_y^2+\frac{i\omega_d(\eta+\nu)}{v_A^2}\frac{\partial^2}{\partial x^2}\}Y^{(n)}\\ &=ik_y\frac{\partial X^{(n)}}{\partial x}+\frac{L}{n\pi}(\frac{\omega_d^2}{v_A^2}-k_y^2)R_y.\end{aligned} \tag{16}$$

It turns out to be convenient to introduce the following quantities

$$\Pi^{(n)} = -(\frac{\partial X^{(n)}}{\partial x}+ik_y Y^{(n)}), \tag{17}$$

$$D_y^{(n)} = \frac{-L}{n\pi}(\omega_d^2-v_A^2k_y^2)R_y, \tag{18}$$

$$\omega_A(x) = v_A(x)\frac{n\pi}{L}. \tag{19}$$

$\Pi^{(n)}$ is related to total pressure, $D_y^{(n)}$ is the driving term due to the footpoint motions and $\omega_A(x)$ is the local Alfvén frequency. With the aid of this notation our main governing equations can be stated as

$$\{\omega_d^2-\omega_A^2(x)-i\omega_d(\eta+\nu)\frac{\partial^2}{\partial x^2}\}X^{(n)} = v_A^2\frac{\partial\Pi^{(n)}}{\partial x}, \tag{20}$$

$$\begin{aligned}\{\omega_d^2-\omega_A^2(x)-i\omega_d(\eta+\nu)\frac{\partial^2}{\partial x^2}\}Y^{(n)} &= ik_y v_A^2\Pi^{(n)}\\ &\quad +D_y^{(n)}.\end{aligned} \tag{21}$$

For $k_y=0$ these equations are decoupled. In that case, the undriven Eq. (20) has the trivial solution $X^{(n)}=0$, whereas Eq. (21) corresponds then to the problem studied by Ruderman et al (1996). In the next section we solve these equations for the Fourier coefficients $X^{(n)}$ and $Y^{(n)}$ for every n and for arbitrary k_y. Once this is done we can reconstruct the full solution from expressions (11) and (13).

3.2. Nonresonant Fourier coefficients

Since the Reynold numbers corresponding to the dissipative coefficients η and ν are extremely large in the solar corona, it is relevant to consider first the ideal case. By dropping the dissipative terms in (20) and (21) and after some reorganisation we obtain

$$\begin{aligned} \frac{\partial \Pi}{\partial x} &= \frac{[\omega_d^2 - \omega_A^2(x)]}{v_A^2} X, \\ \frac{\partial X}{\partial x} &= -\Pi + \frac{v_A^2 k_y^2 \Pi - i k_y D_y}{[\omega_d^2 - \omega_A^2(x)]}, \\ Y &= \frac{i}{k_y}(\Pi + \frac{\partial X}{\partial x}), \end{aligned} \tag{22}$$

where we have dropped the superscripts n. For those Fourier coefficients $X^{(n)}$ and $Y^{(n)}$ for which n is such that

$$[\omega_d^2 - \omega_A^2(x)] = [\omega_d^2 - (v_A(x)\frac{n\pi}{L})^2] \neq 0,$$

these equations can be integrated numerically without any problem. These Fourier coefficients are nonresonant and including dissipation or not in their calculation does not make any difference in practice.

However, it is not very likely that this condition is satisfied for all n at all x, and as a matter of fact there is not a lot of interest in that case. What is likely to happen is that there is at least one $n = n_0 \in N_0$ for which the range

$$[\frac{\pi n_0}{L}\min v_A(x) \ , \ \frac{\pi n_0}{L}\max v_A(x)] \tag{23}$$

contains the driving frequency ω_d of the footpoint motion. In that case there is a position $x = x_A$, given by

$$\omega_d^2 = \frac{\pi^2 n_0^2 v_A^2(x_A)}{L^2} \tag{24}$$

where the ideal solution diverges. This is a consequence of the fact that we did not take dissipation into account which would temper the large gradients around the resonant surface.

To proceed we thus assume that all non-resonant $X^{(n)}$ and $Y^{(n)}$ have been obtained by direct numerical integration of the ideal equations (22). For resonant Fourier coefficients a more subtle procedure including dissipation is needed. In what follows we assume that only the $n = 1$ contribution is resonant and that this contribution is resonant at only one position $x = x_A$. This does not really limit generality since extensions to multiple resonances is a trivial matter in our linear approach.

3.3. Resonant Fourier coefficients

Eqs. (20) and (21) form together with expression (17) a complicated system of differential equation. This difficulty will be solved with a mathematical technique (hereafter the SGHR-method) based on matched asymptotics. It hase been shown (Stenuit, Erdelyi and Goossens 1995) that this, in principle, very simple technique allows for an accurate calculation of resonant

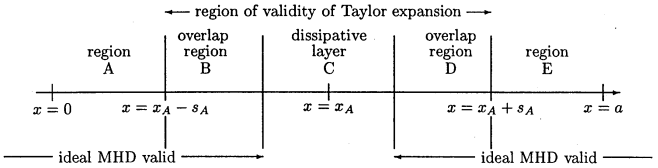

Fig. 2. A schematic overview of the notations used when treating the solution in the dissipative layer.

Alfvén waves in 1D magnetic flux tubes. We refer to Goossens, Ruderman and Hollweg (1995) and Goossens and Ruderman (1995) for a description of the more technical details which we have omitted here for brevity.

We have seen in the preceding subsection that neglecting dissipative terms causes problems around the position $x = x_A$ where the driving frequency equals the local Alfvén frequency for $n = 1$. Following the lines of the SGHR-method, we focus on this position by using the linear Taylor polynomial of $\omega_d^2 - \pi^2 v_A^2(x)/L^2$ around the resonant point $x = x_A$:

$$\omega_d^2 - \pi^2 v_A^2(x)/L^2 = (x - x_A)\Delta + \cdots = s\Delta + \cdots \ , \tag{25}$$

where

$$\Delta = \frac{d}{dx}\left(\omega_d^2 - \frac{\pi^2 v_A^2}{L^2}\right)\Big|_{x=x_A} \ , \tag{26}$$

and $s = x - x_A$. We assume that this linear Taylor polynomial is an accurate approximation of the actual function in the interval $[x_A - s_A \ , \ x_A + s_A]$.

Dissipation removes the ideal singularity from Eqs. (20) and (21) and leads to the appearance of a thin dissipative layer embracing the ideal resonant surface. Due to the very large Reynolds numbers in the solar corona, the thickness of the resonant layer δ_A is in general much smaller than the range of validity s_A of the Taylor expansion. This is important since it implies that in addition to the dissipative layer there are two overlap regions to the left and the right of the dissipative layer contained in the interval $[x_A - s_A \ , \ x_A + s_A]$ (see Fig. 2) where ideal MHD is valid too.

The linear Taylor polynomial for the function $\omega_d^2 - \pi^2 v_A^2/L^2$ is now used to obtain a simplified version of equations (20) and (21) for $n = 1$ valid in the interval $|x - x_A| \lesssim s_A$. By performing the appropriate eliminations we arrive at

$$\begin{aligned} \{\Delta s - i\omega_d(\eta + \nu)\frac{\partial^2}{\partial s^2}\}\frac{\partial X}{\partial s} &= (v_A^2 k_y^2 - \Delta s)\Pi \\ &\quad - i k_y D_y, \end{aligned} \tag{27}$$

$$\{\Delta s - i\omega_d(\eta + \nu)\frac{\partial^2}{\partial s^2}\}Y = i k_y v_A^2 \Pi + D_y, \tag{28}$$

$$\{\Delta s - i\omega_d(\eta + \nu)\frac{\partial^2}{\partial s^2}\}\frac{\partial \Pi}{\partial s} = 0, \tag{29}$$

where v_A^2 is evaluated at $x = x_A$.

The second terms in the lefthand side of equations (27) and (28) are dissipative corrections to the resonant solutions X and

Y. Dissipation plays a role of significance only when the second term is comparable in absolute value to the first term. This results in a dissipative layer of which the thickness is measured by the quantity

$$\delta_A = \left| \frac{\omega_d(\nu + \eta)}{\Delta} \right|^{1/3} . \tag{30}$$

Knowing that the type of equations of (27), (28) and (29) has been encountered before by e.g. Goossens et al. (1995) and Tirry & Goossens (1996) it is now easy to determine the solutions to be

$$\begin{aligned} X &= \frac{-k_y}{\Delta}\alpha G(\frac{s}{\delta_A}) - \Pi s + C_x, \\ Y &= \frac{1}{\delta_A|\Delta|}\alpha F(\frac{s}{\delta_A}), \\ \Pi &= \Pi(s=0), \end{aligned} \tag{31}$$

where C_x is an integration constant and we have defined the complex quantity

$$\alpha = (k_y v_A^2 \Pi - iD_y). \tag{32}$$

$F(\tau)$ and $G(\tau)$ are the universal functions

$$F(\tau) = \int_0^\infty \exp(ik\tau \mathrm{sign}(\Delta) - k^3/3)\, dk \tag{33}$$

$$G(\tau) = \int_0^\infty e^{\frac{-k^3/3}{k}} \{\exp(ik\tau \mathrm{sign}(\Delta)) - 1\}\, dk. \tag{34}$$

Boris (1968) was the first to introduce the $F(\tau)$ function. Goossens et al. (1995) used both functions in their analytical study of linear resonant Alfvén waves in flux tubes that are excited by lateral driving. Wright & Allan (1996) showed in a study on resonant Alfvén waves in magnetospheric conditions that the analytical structure embodied in these functions is fairly insensitive to the details of the dissipation mechanism. The term 'universal function' is therefore appropriate.

Following the SGHR method we can now calculate resonant Fourier coeffiecients as follows. In regions A and B (see Fig. 2) no resonance is encountered and ideal MHD describes the physical picture very well. We can therefore, integrate in this region the equations (22) numerically. As starting value for the variable X we can use the rigid wall boundary conditions ($X(x = 0) = 0$), while for the variable Π the starting value has to be guessed iteratively (see further). Integrating numerically up to the the overlap region B where our anayltically determined dissipative solution (31) is valid, we can now match the unknown integration constant C_x to the numerical solution. This analytically determined dissipative solution (31) is then used to cross the dissipative layer in region C and we arrive in region D, where we use this dissipative solution (31) as starting value for the remaining numerical integration through region E. Finally, the value for the variable X which we find at $x = a$ will in general not match with the required rigid wall boundary condition, but in an iterative shooting procedure we can adjust the guessed starting value $\Pi(x = 0)$ such that $X(x = a)$=0 is fulfilled.

4. Energetics

Now that we have determined the stationary behaviour of the excited waves inside and outside the dissipative layer we can study the resulting dissipation of the wave energy in the coronal loop due to the resonance. In the steady state the energy that enters the loop through the surface $z = 0$ averaged over a period of the driving frequency, must be balanced by the averaged energy dissipated in the resonant layer. As the z component of the velocity is equal to zero at $z = 0$, the time averaged energy flux through the surface $z = 0$ is given by the z-component of the time averaged Poynting vector $\mathbf{E} \times \mathbf{B}^*/2\mu$ integrated over this surface

$$S = \int_0^a [\frac{Re(\mathbf{E} \times \mathbf{B}^*)_z}{2\mu}]_{z=0}\ dx, \tag{35}$$

where $Re(.)$ denotes the real part of a complex quantity, and an '*' its complex conjugate.

With the use of Ohm's law we easily get

$$\frac{1}{2\mu}\mathbf{E} \times \mathbf{B}^* = \frac{1}{2\mu}[\mathbf{v}|B|^2 - \mathbf{B}(\mathbf{v} \cdot \mathbf{B}^*)] + \frac{\eta}{2\mu}(\nabla \times \mathbf{B}) \times \mathbf{B}^* . \tag{36}$$

Taking into account that $v_z = 0$ at $z = 0$ we obtain

$$\begin{aligned} \frac{1}{2\mu}(\mathbf{E} \times \mathbf{B}^*)_z = &- \frac{1}{2\mu}B_0(v_x B_x^* + v_y B_y^*) \\ &- \frac{\eta}{2\mu}(B_x^*\frac{\partial B_x}{\partial z} + B_y^*\frac{\partial B_y}{\partial z}) . \end{aligned} \tag{37}$$

In what follows we denote the magnetic Reynolds number as R_m. The ratio of the second term in the right-hand side of Eq. (37) to the first term is of the order of $\eta/v_A L = R_m^{-1}$ both inside and outside the dissipative layer. Since $R_m \gg 1$, this estimate enables us to neglect the second term in the right-hand side of Eq. (37) in comparison with the first term. The z-component of the time averaged Poynting flux S can then be written as

$$S = -\frac{B_0}{2\mu}\int_0^a Re(v_x B_x^* + v_y B_y^*)dx . \tag{38}$$

The quantities v_x, v_y, B_x and B_y in Eq. (38) are calculated at $z = 0$. Since we impose a purely azimuthal footpoint driving, we have $v_x = 0$ at $z = 0$ and the first term in expression (38) drops out. Expressing v_y and B_y in terms of the displacement component ξ_y results in

$$S = \frac{\omega_d}{2}\int_0^1 Re(i\xi_y\frac{\partial \xi_y^*}{\partial z})dx, \tag{39}$$

where we wrote S now in nondimensionalised form. Finally, by recalling that ξ_y is given by the footpoint motion (8) at $z = 0$ and that only the resonant Fourier coefficient for $n = 1$ has an imaginary part we arrive at

$$S = \omega_d R_y \frac{\pi}{L^2}\int_0^1 Im(Y^{(1)})dx, \tag{40}$$

where $Im(.)$ denotes the imaginairy part. Since in a stationary state no energy stock can be built up in the loop, S also equals the heating rate in the loop. In addition, it will be interesting to examine also the Poynting flux which enters the resonant layer *directly* at its photospheric base

$$S_{dir} = \omega_d R_y \frac{\pi}{L^2} \int_{res.layer} Im(Y^{(1)}) dx. \quad (41)$$

The difference

$$S_{ind} = S - S_{dir} \quad (42)$$

is the energy flux that enters the loop through the $z = 0$ plane, but outside the base of the resonant layer. Since only the dissipative layer can act as a sink of energy (by conversion to heat, of course), all the energy flux S_{ind} that goes to the non-resonant part of the loop, has to leave it again which it can only do sideways into the dissipative layer. As such, S_{ind} is the energy flux entering the dissipative layer sideways and is refered to as the *indirect* energy flux. Note that the total energy flux S must be positive (i.e. into the loop), while the direct S_{dir} and the indirect S_{ind} energy flux can be negative (as long as their sum is positive).

5. Results

As an instructive example, rather than a realistic model, we look at a loop with dimensions $L = 1$ and $a = 1$. In this case the phenomena under investigation manifest themselves the clearest. We have also taken $(\eta + \nu) = 10^{-6}$ which is possibly too high for the solar corona, but which has the advantage that it yields sufficiently wide dissipation layers so that the wave structure is clearly visible on the pictures. By taking appropriate values for ρ_A and ρ_B in expression (1) we can control the width of the Alfvén continuum and determine whether or not a quasi-mode is present in the continuum for $n = 1$. Once ρ_A and ρ_B are specified we are left with the two free parameters, ω_d and k_y, which determine the footpoint driving (8) (note that the constant R_y is only a scaling factor in our linear approach). We first focus in the next subsection on the case without a quasi-mode in the $n = 1$ continuum, while in the following subsection we look at the modifications induced by the presence of a quasi-mode. In each case we investigate the wave heating as a function of the footpoint parameters (ω_d, k_y).

5.1. In the absence of a quasi-mode

We take $\rho_A = 0.8$ and $\rho_B = 0.2$. This results in a range of Alfvén frequencies in the $n = 1$ continuum from $\omega = \pi$ at $x = 0$ up to $\omega = 4.06$ at $x = 1$ (all in dimensionless units). No discrete eigenfrequency was found in this frequency range.

In Fig. 3 we show the wave structure as a function of x at a height $z = L/2$ for $\omega_d = 3.58$ and $k_y = 0.5$. For these values of the driving frequency and the azimuthal wave number, the quantity α (32) turns out to be a purely imaginairy number. As a consequence, the real (smoothed out $\ln(x)$-function) and imaginary part (Heaviside jump-function) of the G-function, and the real (smoothed out δ-function) and imaginary part (smoothed out $1/x$-function) of the F-function can immediately be recognised (see Goossens, Ruderman & Hollweg 1995). It is clear that driving at the footpoints does not alter qualitatively the structure of the wave dynamics in the resonant layer as compared to sideways driving.

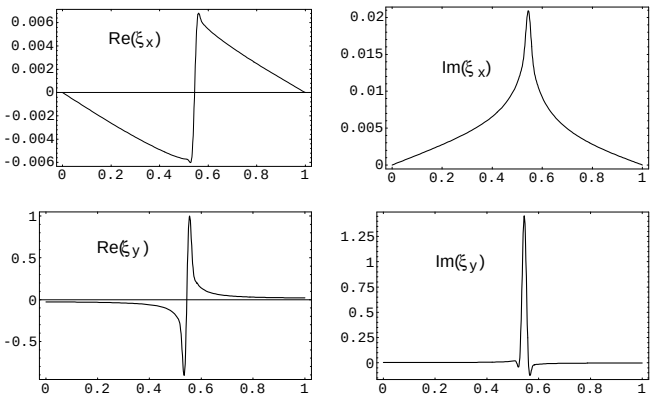

Fig. 3. The ξ_x and ξ_y components as a function of x, induced by a footpoint motion with characteristics (ω_d, k_y)=(3.58,0.5). The wave structure is shown at a height $z = L/2$.

Different values for ω_d and k_y result in complex values for the quantity α (32) which 'mixes' the real and imaginairy parts of the F and G function and leads to less instructive pictures then Fig. 3. More important however is the change of the magnitude of α as a function of ω_d and k_y. This has profound effects on the time averaged energy input in the loop given by the Poynting flux S (40) shown in Fig. 4.

In Fig. 4, the frequency ω_d (horizontal axis) ranges from $\omega_d = 3.16$ up to $\omega_d = 4.00$ so that both the far-left and the far-right wing of the $n = 1$ continuum are not displayed. Fig. 4 shows clearly an increasing Poynting flux when approaching these extremes. This is a consequence of the flatness of the density profile, and consequently of the Alfvén frequency profile, around $x = 0$ and around $x = a$. This causes $\Delta \rightarrow 0$ (see expression (26)) and as result $X^{(1)}$ and $Y^{(1)}$ (31), which are proportional to $1/\Delta$, diverge leading to a diverging Poynting flux. These enhanced Poynting fluxes are however not interesting from a physical point of view: it is well-known (see e.g. Mann, Wright and Cally 1995) that the typical time scale on which small length scales are created is proportional to $1/\omega'_A(x)$ which becomes formally infinite for a flat profile. As a consequence, this kind of resonances never leads to dissipation within a typical lifetime of a coronal loop.

A second observation which can be made from Fig. 4 is the fast decay of the Poynting flux S (40) for increasing k_y. To investigate this decay more in detail we have made Fig. 5 as a vertical cross-cut of Fig. 4 for $\omega_d = 3.58$. In addition we have also drawn the time averaged Poynting fluxes through the photospheric base of the resonant layer S_{dir} (41) and its complement S_{ind} (42). This picture can be understood as follows. When $k_y = 0$, different magnetic surfaces are perfectly decoupled and the dissipative layer can only get energy input from

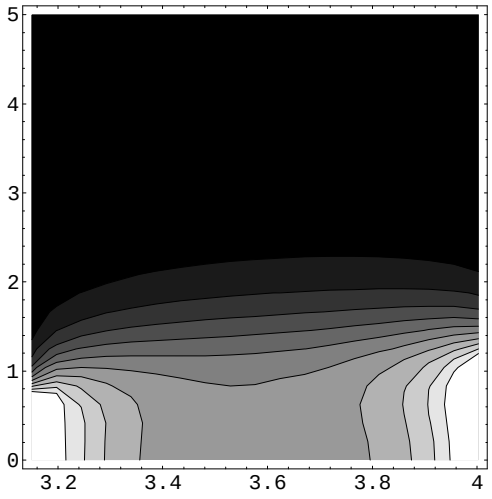

Fig. 4. Contourplot of the Poynting flux S as a function of driving frequency ω_d (horizontally) and azimuthal wave number k_y (vertically) for the equilibrium without a quasi-mode in the n = 1 continuum.

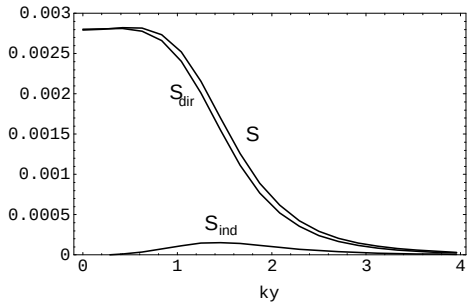

Fig. 5. The Poynting flux S, S_{ind} and S_{dir} as a function of the azimuthal wave number k_y and evaluated for a driving frequency ω_d = 3.58

its photospheric base resulting in $S = S_{dir}$ and $S_{ind} = 0$. For $k_y \neq 0$ however, the magnetic surfaces are coupled and energy can now also enter or leave the dissipative layer sideways. As a consequence, S_{dir} decays (wave energy is not perfectly contained in the dissipative layer anymore) and S_{ind} grows (wave energy can enter the dissipative layer sideways). For $k_y \sim 1.4$ this coupling is 'optimal'. For larger k_y also the indirect flux S_{ind} approaches zero.

It is no surprise that the sideways contribution S_{ind} remains small compared to S_{dir}. The contribution S_{ind} corresponds to 'fast wave'-behaviour, since Alfvén waves propagate their energy strictly along the magnetic field. 'Fast mode'-behaviour is however not supported at the frequency ω_d = 3.58 by the chosen equilibrium (remember we have taken the values for ρ_A and ρ_B in order to avoid the presence of a quasi-mode). This results in a small S_{ind} contribution.

5.2. In the presence of a quasi-mode

We now take ρ_A = 0.6 and ρ_B = 0.4. This results in a range of Alfvén frequencies in the n = 1 continuum from $\omega = \pi$ at x = 0 up to ω = 7.02 at x = 1 (all in dimensionless units).

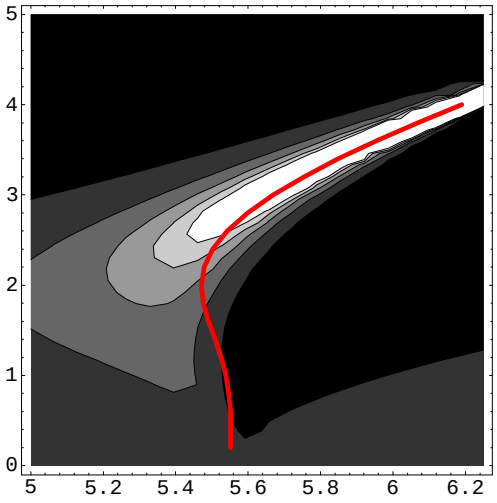

Fig. 6. The Poynting flux S as a function of the driving frequency ω_d (horizontally) and the azimuthal wave number k_y (vertically). Also indicated in these pictures is the position of the quasi-mode frequency by a thick grey line.

We determined the presence of a quasi-mode in this n = 1 continuum at a frequency [1] ω_q = 5.551 for k_y = 0 (see Tirry & Goossens, 1996 for a description of the method used). From a global point of view, the dependence of the Poynting flux S remained the same as in the previous subsection (see Fig. 4): a decrease for large k_y and physically unimportant peaks towards the left and right wing of the continuum.

However, in the neighbourhood (in (ω_d, k_y) space) of the quasi-mode frequency the appearance of the Poynting flux S changes dramatically. In Fig. 6 we show the quasi-mode frequency as a grey line superimposed on a contourplot of the time averaged Poynting flux S as a function of driving frequency ω_d (horizontally) and azimuthal wave number k_y (vertically). The correspondence of (ω_d,k_y)-values of very enhanced Poynting fluxes, with the position of the quasi-mode frequency line is striking at least for $k_y > 2.5$. For small values of k_y this correspondence is less clear.

Another peculiar phenomenon is the large dark area to the right of the quasi-mode frequency line. This is a 'valley' of combinations of ω_d and k_y for which footpoint driving leads to only a very small Poynting flux S. Although the Poynting flux S remains positive everywhere in this region, there is a line in the middle of this valley where the Poynting flux S approaches zero. This line, which we will hereafter call the 'anti-resonance line', re-appears in Fig. 7. In this figure we show a kind of primitive contourplots of S_{ind} (left) and S_{dir} (right): light regions correspond to positive values and dark regions correspond to negative values. This means that region I corresponds to (ω_d, k_y)-values giving $S_{ind} < 0$ and region II corresponds to (ω_d, k_y)-values

[1] In this paper we refer by quasi-mode frequency actually to the real part of the quasi-mode frequency. The imaginairy part of the quasi-mode frequency -the damping rate- is less important in the present discussion.

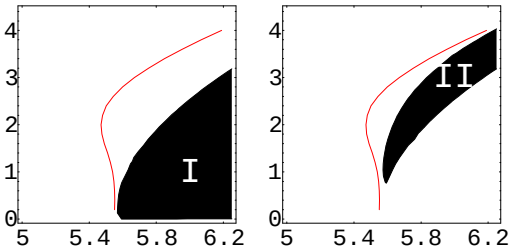

Fig. 7. The S_{ind} (left) and S_{dir} (right) as a function of the driving frequency ω_d (horizontally) and the azimuthal wave number k_y (vertically). Light regions correspond to positive values and dark regions to negative values. The position of the quasi-mode frequency is indicated by a thick grey line.

giving $S_{dir} < 0$. Note that region I and II do not overlap (as they should since $S = S_{ind} + S_{dir} \geq 0$) but that they apparently have a common boundary where $S_{ind} \equiv 0$ and $S_{dir} \equiv 0$, and as a consequence $S \equiv 0$. This boundary is the above baptized anti-resonance line. From a physical point of view we do not expect that S becomes exactly zero for some (ω_d, k_y)-value, since this would lead to the strange conclusion that there is no energy dissipation at all in our dissipative system. In this context it is important to remember our approximation that dissipation is only retained in the neighbourhood of the resonant layer. Although this approximation is valid for all practical purposes one can expect a very small, yet finite dissipation in the whole plasma volume leading to a Poynting flux S which is strictly positive.

Note that the anti-resonance line approaches the quasi-mode frequency line for decreassing k_y. This might be the reason why enhanced Poynting fluxes S in Fig. 6 are not nicely coinciding with the quasi-mode frequency line for small k_y.

These results were obtained for a 'square' loop (i.e. $L = 1$ and $a = 1$) and one can wonder about their significance for the solar reality. However, doing the same excercise for a model of a coronal loop with realistic aspect ratios results in much complexer situations where different Alfvén continua can overlap and probably a large number of quasi-modes is present. We preferred therefore to focus on the simplest situation conceivable in order to enlighten the new physical phenomena the clearest.

6. Interpretation

In the preceeding section we have seen that the driving of a coronal loop by azimuthally polarised footpoint motions results in a complicated picture of energy flows in and out the dissipative layer, especially in the presence of quasi-modes. In this section we will try to enlighten this last situation. Fig. 8 shows a vertical cross-cut of Fig. 7 at a frequency $\omega_d = 6.00$. The panel at the lefthandside shows the total energy flux S as a function of k_y while the panel at the righthandside shows the indirect S_{ind} and direct energy fluxes S_{dir} as a function of k_y. The same cross-cut is shown symbolically with a set of cartoons in Fig. 9.

Let us start with the combination $(\omega_d, k_y) = (6.00, 0)$ in Fig. 8 and Fig. 9. For $k_y = 0$ the different magnetic surfaces are decoupled and the dissipative layer can only be fed directly

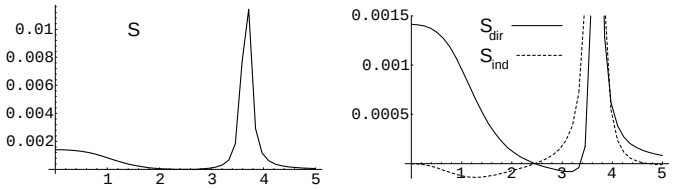

Fig. 8. The total energy flux S (left) and the indirect S_{ind} and direct energy flux S_{dir} (right), all as a function of k_y and evaluated for a driving frequency $\omega_d = 6.00$.

from its photospheric base. As a consequence we have $S_{ind} = 0$ and $S = S_{dir} > 0$.

For increasing k_y we now enter the region I of Fig. 7 where S_{ind} is negative. and S_{dir} is positive (see also Fig. 8a). Region I corresponds to combinations of (ω_d, k_y) where there is an energy inflow at the photospheric base of the dissipative layer which is partly dissipated in this layer but partly also escapes again back into the photosphere outside the dissipative layer. This means that the coupling of the different magnetic surfaces results in a sideways energy leakage out of the resonant layer (see second cartoon of Fig. 9).

As we increase k_y up to around 2.5 we cross in Fig.7 the boundary of region I and region II: the anti-resonance line. This is clearly seen in Fig. 8 where both S_{ind} and S_{dir} change sign. As a result the time-averaged total energy input S is neglibible in the whole range $k_y \in [2, 3]$. In the companion paper the anti-resonance line is recovered in the time-dependent approach. There, the anti-resonance line is explained in terms of being those (ω_d, k_y) combinations for which the Alfvén waves excited directly at the photospheric base of the dissipative layer or in perfect anti-phase with the Alfvén waves excited through coupling with fast waves.

As we keep on increasing k_y beyond the encounter with the anti-resonance line, we now enter the region II of Fig. 7 where S_{dir} is negative and S_{ind} is positive (see also Fig. 8b). In region II the energy flow is reversed as compared to region I: a large energy inflow is present through the $(z = 0)$ plane excluding the base of the dissipative layer. This energy enters the dissipative layer sideways where its mayor part is dissipated while a small fraction escapes again through the base of the dissipative layer, back into the photosphere.

For $k_y \approx 3.7$ we cross the quasi-mode frequency line in Fig. 6. The total energy input S raises spectacular which is no surprise because S_{dir} and S_{ind} show both a strong positive peak (Fig. 8).

7. Summary and conclusions

In this paper we investigated the excitation of resonant Alfvén waves in coronal loops by azimuthally polarised motions of the photospheric footpoints of the fieldlines. Since our main interest was to obtain qualitative information on the new wave physics owing to $k_y \neq 0$, we focussed on a very simple model for a coronal loop. We considered a straight, static slab model

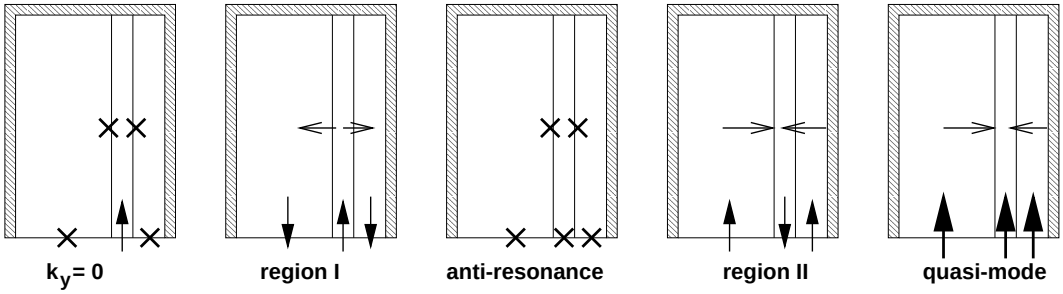

Fig. 9. A set of cartoons symbolising (from left to right) the different energy flow patterns when following a vertical path (from bottom to top) through Fig. 6. at a driving frequency ω_d = 6.00. A coronal loop is symbolically drawn as a rectangle where the lower edge (at which we apply the footpoint motion) is permeable for energy fluxes. The two vertical lines inside the loop denote the edges of the dissipative layer around the resonance. Energy fluxes are shown as arrows. In case of a vanishing energy flux we have drawn crosses.

filled with a pressureless plasma obeying the equations of visco-resistive, linear MHD.

With the help of the SGHR-method we were able to integrate these equations and found the wave solution in the stationary state as a function of the driving frequency ω_d and the azimuthal wave number k_y imposed by the footpoint motion. On the magnetic surface where the driving frequency ω_d equals the local Alfvén frequency, the solution diverges in ideal MHD. When resistivity and viscosity are included, the ideal singularity is removed and replaced by a dissipative layer where gradients are large but finite. In addition, we derived expressions for the energy flux entering the dissipative layer through its photospheric base and the energy flux entering the dissipative layer sideways. The sum of these two is the total energy flux delivered by the footpoint motions and dissipated in the coronal loop.

These expressions turned out to be valuable tools for the investigation of the stationary heating of the coronal loop as a function of the footpoint characteristics (ω_d, k_y). For $k_y = 0$, as it was studied in previous papers, the different magnetic surfaces live in splendid isolation and the dissipative layer can only obtain energy input directly from its photospheric base. When the azimuthal wave number $k_y \neq 0$ the different magnetic surfaces become coupled and energy can now also flow sideways in and out the dissipative layer. In the absence of a quasi-mode this effect is always positive in the sense that the energy is now not only entering the dissipative layer from below (at its photospheric base) but also sideways. For larger k_y the energy entering the loop, and thus the heating, goes to zero.

If however a quasi-mode is present the dependence of the heating on the driving frequency ω_d and the poloidal wave number is drastically changed. For (ω_d, k_y) corresponding to the quasi-mode the heating is enhanced by several orders of magnitude. This is an unexpected result since, in contrast to a sideways driven loop, a loop driven at the footpoints by azimuthally polarised footpoint motions does not need the quasi-modes as energy carrier waves. In the presence of a quasi-mode the coupling of different magnetic surfaces does not always have a positive effect on the heating: we found regions in (ω_d, k_y)-space where not all of the energy entering the dissipative layer is actually dissipated but partly escapes again sideways. In addition, we found a so-called 'anti-resonance' in (ω_d, k_y)-space at which no energy is dissipated in the loop at all though we do drive with a frequency within the Alfvén continuum. At this stage we cannot explain the physics of the anti-resonance.

It seemed therefore necessary to take a closer look on these unexpected phenomena from a fresh point of view. This is done in the companion paper II where we reconsider the same problem but using a time-dependent, ideal approach. The results of paper II do not only confirm our findings, but in addition provide a physical insight in the above introduced regions I and II and the anti-resonance line.

Acknowledgements. The authors greatfully acknowledge the suggestion by M. Goossens to look at this problem. Various discussions with S. Poedts and M. Ruderman were of valuable help.

References

Berghmans, D., & De Bruyne, P., 1995, ApJ, 453, 495.
Berghmans, D., De Bruyne, P., & Goossens, M., 1996, ApJ, 472, 398.
Boris, J.P., 1968, 'Resistive modified normal modes of an inhomogeneous incompressible plasma', Ph.D. Thesis Princeton University, UMI Dissertation Services, Ann Arbor Michigan, p. 172.
Davila, J.M., 1987, ApJ, 317, 514.
Goossens, M., 1991, in E.R.Priest and A.W.Hood (eds.),'MHD Waves and Wave Heating in Non-Uniform Plasmas', *Advaces in Solar System Magnetohydrodynamics*, Cambridge University Press, Cambridge, p. 135.
Goossens, M. & Ruderman, M.S., 1995, Phys. Scripta, T60, 171.
Goossens, M., Ruderman, M.S., & Hollweg, J.V., 1995, Solar Phys., 157, 75.
Halberstadt G. & Goedbloed, J.P., 1995a, A&A, 301, 559
Halberstadt G. & Goedbloed, J.P., 1995b, A&A, 301, 577
Heyvaerts, J. & Priest, E.R., 1983, A&A,117, 220
Hollweg, J.V., 1990, Computer Phys. Rep., 12, 205.
Hollweg, J.V., 1991, in P.Ulmschneider, E.R.Priest and R.Rosner (eds.), 'Alfvén Waves', *Mechanisms of Chromospheric and Coronal Heating*, Springer-Verlag, Berlin, p. 423.
Kuperus, M., Ionson, J.A., & Spicer, D., 1981, Ann. Rev. Astron. Astrophys., 19, 7.
Mann, I.R., Wright, A.N., & Cally, P.S. 1995, J. Geophys. Res., 100, 19441
Ofman L., Davila, J.M. & Steinolfson R.S, 1995, ApJ, 444, 471.

Poedts, S., & Boynton, G.C., 1996, A&A, 306, 610.
Ruderman, M.S., Berghmans, D., Goossens, M., & Poedts, S. 1996, A&A, accepted
Saba, J.L.R., & Strong, K.T. 1991, ApJ, 375, 789
Stenuit, H., Erdélyi, R. & Goossens, M. 1995, Solar Phys., 161, 139.
Tirry, W.J. & Goossens M., 1996, ApJ, 471, 501
Tirry, W.J. & Berghmans, D. 1997, A&A, this issue
Tirry, W.J., Berghmans, D., & Goossens, M. 1997, A&A, accepted
Ulrich, R.K. 1996, ApJ, accepted
Wright, A.N. & Allan W., 1996, JGR, 101, 17399.
Wright, A.N., & Rickard, G.J. 1995, ApJ, 444, 458

This article was processed by the author using Springer-Verlag LaTeX
A&A style file *L-AA* version 3.